Contents lists available at ScienceDirect

Electrochemistry Communications

journal homepage: www.elsevier.com/locate/elecom

Highly sensitive and disposable screen-printed ionic liquid/graphene based electrochemical sensors

Wichayaporn Kamsong, Vitsarut Primpray, Patiya Pasakon, Chakrit Sriprachuabwong, Saithip Pakapongpan, Johannes Philipp Mensing, Anurat Wisitsoraat, Adisorn Tuantranont, Chanpen Karuwan *

Graphene Sensor Laboratory (GPL), Graphene and Printed Electronics for Dual-Use Applications Research Division (GPERD), National Security and Dual-Use Technology Center (NSD), National Science and Technology Development Agency (NSTDA), Phahonyothin Road Khlong Nueng, Khlong Luang, Pathum Thani 12120, Thailand

ARTICLE INFO

ABSTRACT

In this work, a highly sensitive and disposable screen-printed ionic liquid-graphene electrode (SPIL-GE) was developed for electrochemical sensing. The paste for screen printing was facilely prepared by mixing IL with electrolytically exfoliated graphene in poly(3,4-ethylenedioxythiophene) polystyrene sulfonate (GP/PEDOT/PSS) and carbon paste (CP) via ball milling. The IL-GP paste was then screen printed to form working and counter electrodes (WE & CE) followed by screen printing of Ag/AgCl reference electrode and insulator layer on a polyethylene substrate. Electrode geometries were optimized for electrochemical sensing, arriving at an optimal design with an overall electrode length of 25 mm, and CE and WE active areas of 15.70 and 12.57 mm^2, respectively. SPIL-GEs employing six ILs with imidazolium and pyridinium cations were assessed for electrochemical sensing of $K_3Fe(CN)_6$. The pyridinium-type IL, namely 3-methyl-1-propylpyridinium bis(trifluoromethyl sulfonyl)imide (PMPlm), was found to exhibit the highest CV peak currents compared with other ILs at an optimal PMPlm content of 1.0% (w/w). Characterization with scanning electron microscopy and Fourier-transform infrared spectroscopy confirmed the presence of PMPlm, GP/PEDOT/PSS and CP in SPIL-GEs. The electrochemical performance of the optimal SPIL-GE towards the three common analytes including ferri/ferro cyanide $(Fe(CN)_6)^{3-/4-}$ redox couple, dopamine and hydroquinone were compared with the screen-printed carbon and graphene electrodes (SPCE & SPGE). From the results, the SPIL-GE demonstrated larger anodic currents with lower oxidation potentials for the three analytes than SPGE and SPCE, respectively. Therefore, the SPIL-GE could be a potential candidate for advanced electrochemical sensing applications.

1. Introduction

Advanced electrochemical sensors with high sensitivity and low detection limits are highly demanded for electrochemical trace analyses. In general, the electrochemical sensing performance depend mainly on the properties of electrode materials and electrode geometry. Graphene, a 2-dimensional (2D) nanocarbon structure, has been considered as a highly effective material for electrochemical applications owing to its large specific surface area, excellent electrical conductivity and high chemical stability [1,2]. It has been employed as a primary electrode material or an additive to promote electron transfer between a target analyte and electrode surface, resulting in high electrochemical sensitivity [3–5]. In particular, screen-printed graphene electrodes (SPGEs)

have been reported to exhibit considerably higher electrochemical response than those of screen-printed carbon electrodes (SPCEs) [3]. Moreover, graphene-based electrodes have been modified with various kinds of materials including conductive polymers [6–8], metal nanoparticles [9–12] and ionic liquids (ILs) [13–18] in order to further enhance their electrochemical performance. Among these, ILs are particularly promising due to wide electrochemical potential window, good solvation ability, low volatility, low toxicity and high chemical stability [19–22]. In addition, ILs have high electrical conductivity since they are liquid-state salt compounds formed by pairing positive and negative ions. Two kinds of ILs containing imidazolium and pyridinium cations have been widely used for electrochemical applications. In particular, SPGEs and SPCEs surface-modified with imidazolium-type

---
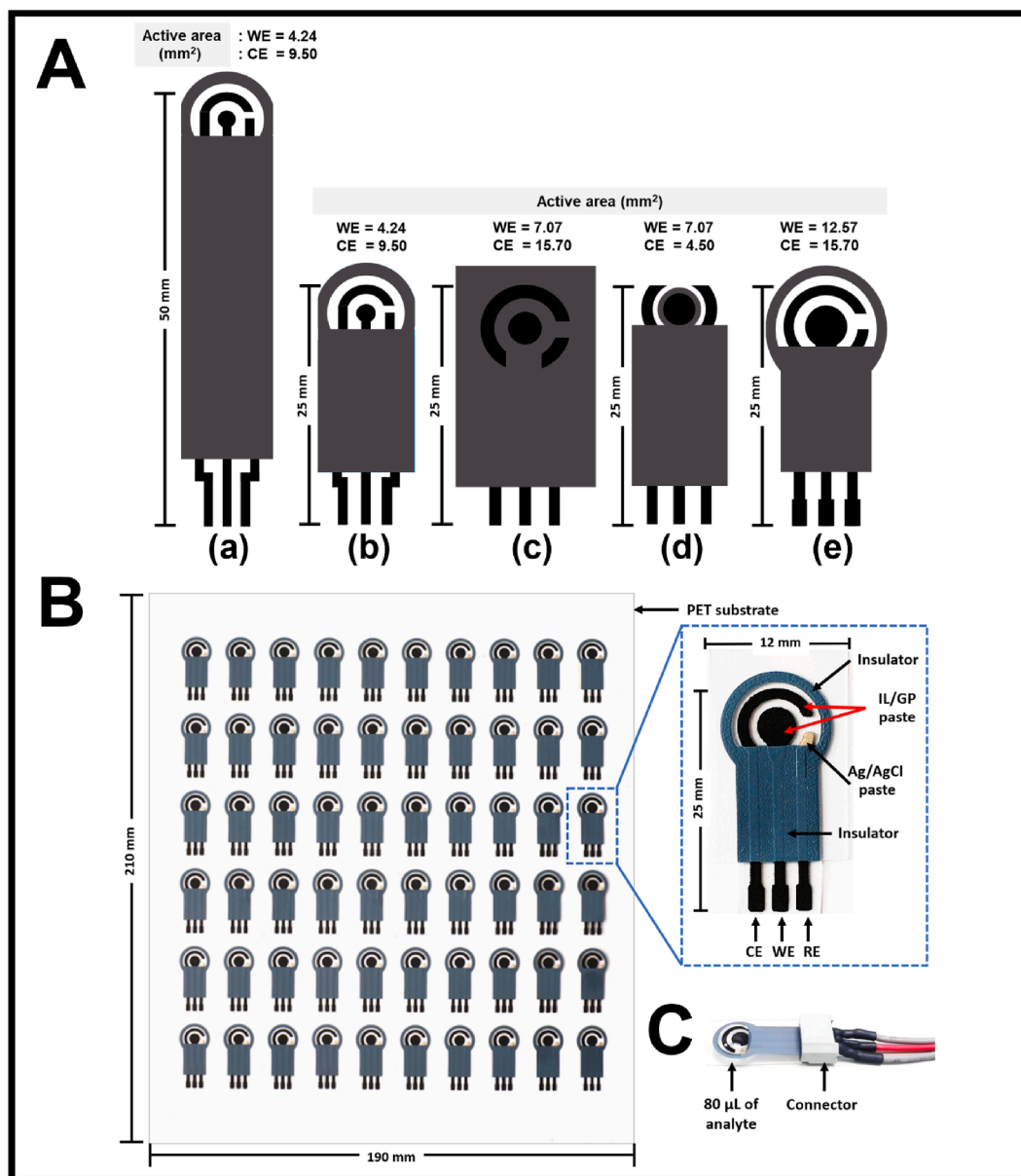
Fig. 1. (A) Five designs of screen printed electrodes and typical photographs of (B) fabricated SPIL-GEs on a single PET substrate (190 × 210 mm^2) and (C) a single SPIL-GE with an electrical connector.

and pyridinium-type ILs have shown significantly improved electrochemical response towards multiple groups of analytes [14,18,23]. It is thus appealing to further develop high-performance electrochemical electrodes based on ILs and graphene. Generally, the characteristics of electrodes depend considerably on the preparation process, which shall also be able to fabricate electrochemical sensors productively and reproducibly at low-cost for industrial use. Screen printing is one of the practical processes that can meet most of these fabrication requirements. Thus, screen-printed electrodes (SPEs) have been extensively applied to electrochemical analyses [24–26]. However, there is no report of electrodes directly fabricated by screen printing of inks containing ILs and GP. The electrodes prepared by screen printing from the mixtures of ILs and GP should be superior to IL-modified SPEs in terms of electrode uniformity, reusability and controllability.

In this work, disposable screen-printed IL/graphene electrodes (SPIL-GEs) were innovatively fabricated using the pastes produced by blending ILs with electrolytically-exfoliated graphene and carbon paste (CP) via ball milling. In addition, one pyridinium-type and five

imidazolium-type ILs were evaluated and IL content was varied in order to maximize the electrochemical sensing performance for detection of three common electroactive analytes including ferri/ferro cyanide (Fe $(CN)_6)^{3-/4-}$ redox couple, dopamine (DA) and hydroquinone (HQ). Additionally, the geometries and sizes of designed electrodes were adjusted to attain optimal electrochemical response.

2. Materials and method

2.1. Chemicals and materials

All chemicals utilized in this work were of analytical grade and used without further purification. Commercial poly(3,4-ethylenedioxythiophene) polystyrene sulfonate (PEDOT/PSS) (Clevios P Jet N from HC Starck, USA) solution was employed as an electrolyte for electrolytic exfoliation. Carbon paste (CP, Item code: C2030519P4), silver/silver chloride paste (Ag/AgCl, Item code: C61003P7) and insulating paste (Item code: D2070423P5) were purchased from Sun
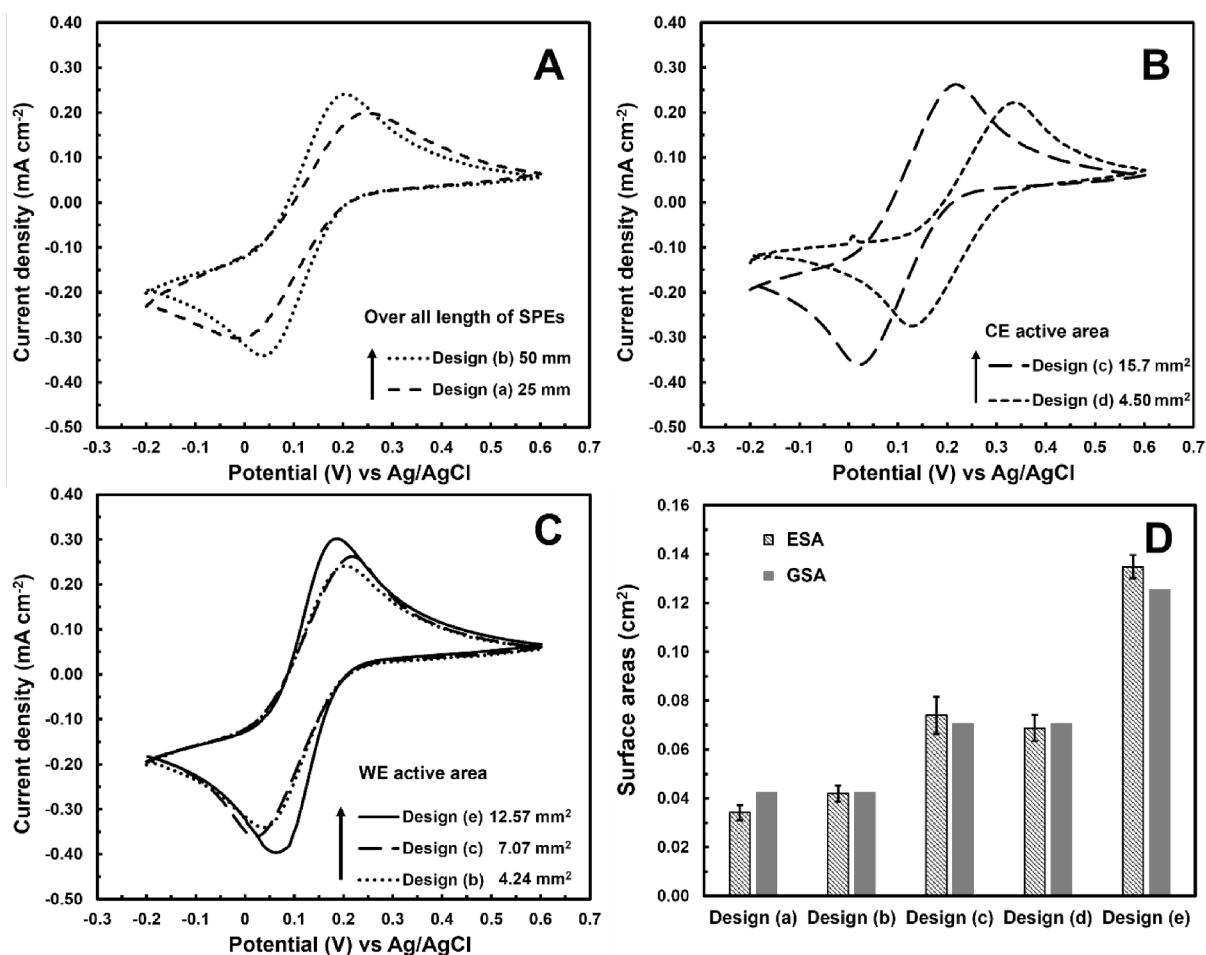
Fig. 2. Cyclic voltammograms of SPGEs with different (A) overall electrode lengths (Designs (a)-(b)), (B) CE active area (Designs (c)-(d)) and (C) WE active area (Designs (b)-(c) and (e)) towards 2.5 mM $K_3Fe(CN)_6$ at 50 mVs^{-1}. (D) Electrochemical and geometric surface areas (ESA & GSA) of SPGEs with different designs.

Chemicals (USA). Standard solutions of potassium hexacyanoferrate (III) $(K_3Fe(CN)_6)$, DA, HQ and phosphate buffer saline (PBS) solutions were acquired from Sigma (USA). ILs including 3-methyl-1-propylpyridinium bis(trifluoromethyl sulfonyl)imide (PMPIm), 1-ethyl-3-methylimidazolium tetrafluoroborate (EMIMBF$_4$), 1-hexal-3-methylimidazolium hexafluorophosphate (HMIMPF$_6$), 1-butyl-3-methylimidazolium hexafluorophosphate (BMIMPF$_6$), 1-butyl-3-methylimidazolium hexafluorophosphate (BMIMBF$_4$) and 1-butyl-3-methylimidazolium thiocyanate (1-butyl-3-methyl-1H-imidazolium thiocyanate) $(C_9H_{15}N_3S)$ were also supplied by Sigma (USA).

2.2. Instruments

A commercial ball mill (Retsch model Emax) was used to mix and homogenize screen-printing inks. A screen printer (DEK model 03ix) was employed to print conductive paste on PET substrates. Cyclic voltammetry (CV) measurements were conducted using a potentiostat (μ-Autolab Type III, Methrom) equipped with GPES program to investigate electrochemical performance. A scanning electron microscope (SEM, Hitachi model S-4700) and Fourier-transform infrared spectroscope (FTIR, Perkin Elmer model spectrum spot light-300) were employed to characterize the morphological and chemical properties of paste materials, respectively.

2.3. IL-GP paste preparation

Graphene powder was synthesized via electrolytic exfoliation by applying a constant voltage of 8 V between two graphite rods immersed in PEDOT/PSS solution (100 ml) for 20 h followed by filtering through a filter paper (Whatman grade 2, 8 μm pore size) to remove large aggregates. IL and electrolytically exfoliated GP/PEDOT/PSS solution were then mixed with the commercial CP with CP:GP/PEDPT/PSS:IL weight composition of 100:2.5:1. One pyridinium-type IL, namely PMPIm, and five imidazolium-type ILs including EMIMBF$_4$, BMIMPF$_6$, HMIMPF$_6$, BMIMBF$_4$, and $C_9H_{15}N_3S$ were employed in this study. In addition, the content of IL providing the highest electrochemical response was varied from 0.5 to 2.0 % (w/w). The three-component mixture were unified into a homogeneous paste by ball milling at 1,000 rpm for 2 h. In the ball milling process, the ball mill jar was tightly sealed and only opened 2 h after ball milling to minimize solvent evaporation. The obtained IL-GP ink was used for screen-printing of working and counter electrodes.

2.4. Electrode design and fabrication

Five geometric designs of electrodes were made with different overall electrode lengths and working electrode (WE) and counter electrode (CE) active areas using Adobe Illustrator as displayed in Fig. 1A. The 1st and 2nd designs ((a)-(b)) comprised WEs with the same WE active area of 4.24 mm^2 but had different overall electrode lengths of 50 mm and 25 mm, respectively. The 3rd and 4th designs ((c)-(d)) had the same WE active area of 7.1 mm^2 and the overall length of 25 mm but distinct CE active areas of 15.7 mm^2 and 4.5 mm^2, respectively. The 5th design (e) exhibited the largest WE active area of 12.57 mm^2 with the same overall and CE active area as those of design (c).

For the fabrication of electrochemical sensors, CP, GP and IL-GP pastes were screen-printed through the first patterned stencil mesh to
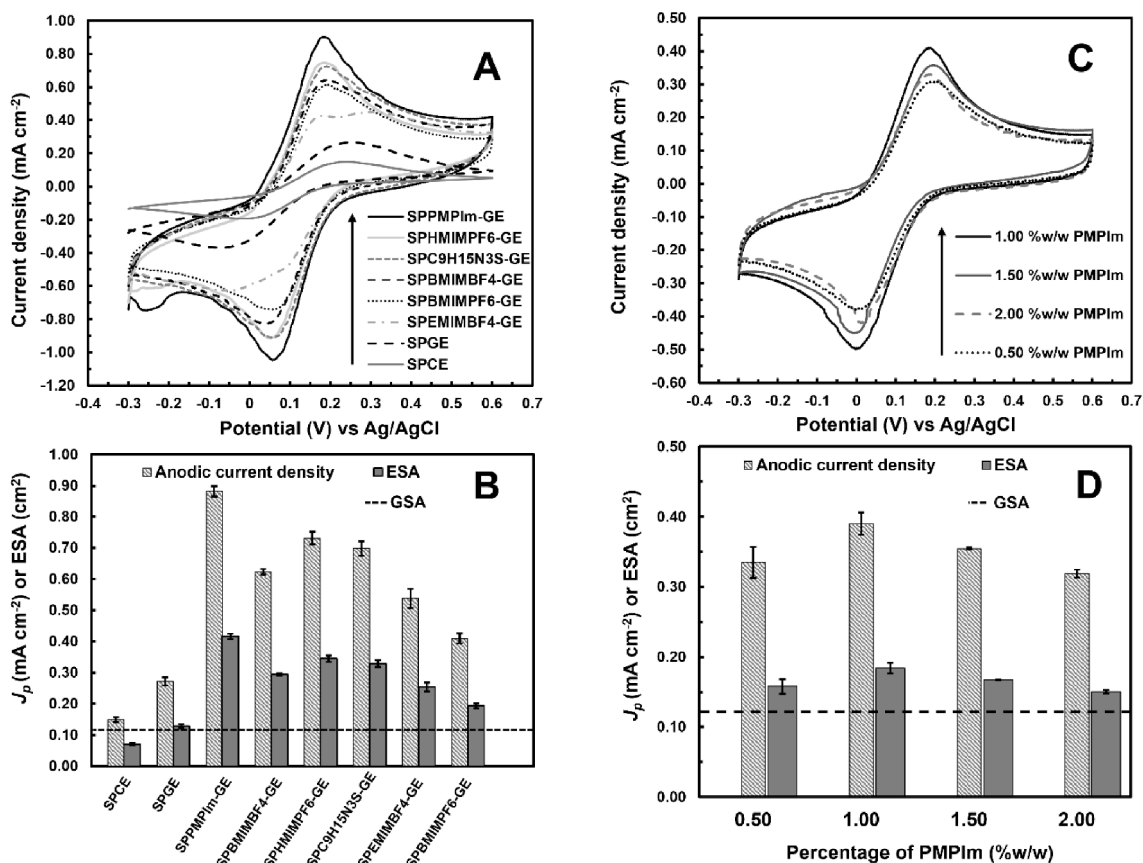
Fig. 3. Cyclic voltammograms of (A) SPCE, SPGE, and SPIL-GEs with different IL materials towards 5 mM K$_3$Fe(CN)$_6$ at 50 mVs^{-1} and (B) corresponding J_p and ESAs. (C) Cyclic voltammograms of SPPMPIm-GEs with different PMPIm contents towards 2.5 mM K$_3$Fe(CN)$_6$ at 50 mVs^{-1} and (d) corresponding J_p and ESAs. The dotted lines in (B) and (D) correspond to the geometric surface area (GSA) of WE.

simultaneously form WE and CE on poly-ethylene terephthalate (PET) substrates. Ag/AgCl and insulator pastes were then successively screen-printed through the second and third patterned meshes under alignments to attain reference electrode (RE) and insulator layer, respectively. The printed substrates were baked at 60 °C for 5 min in an oven to remove solvents after printing each electrode layer and finally dried at 120 °C for 5 min upon printing the insulator layer. The sensors made from CP, GP and IL-GP were labeled as SPCEs, SPGEs and SPIL-GEs, respectively. The general term IL might be substituted with the name of a specific IL.

2.5. Electrochemical measurement

The printed electrodes were connected to the potentiostat via an electrical connector as shown in Fig. 1C and then electrochemically cleaned to remove contaminants on electrode surfaces in 0.1 M PBS solution (pH 7.4) by applying voltage between −0.3 and + 0.6 V in cyclic voltammetry (CV) mode for 5 cycles at a scan rate of 50 mVs^{-1}. 80 μl of analyte was dropped on the sensing area before running CV scans. CV measurements were conducted towards 2.5–5 mM K$_3$Fe(CN)$_6$, 1 mM DA and 1 mM HQ in 0.1 M PBS solution (pH 7.4) at a fixed scan rate of 50 mVs^{-1}. The electrochemical sensors employed in this study included SPIL-GEs, SPGEs, SPCEs and two commercial SPEs, namely SPGE-E1 and SPCE-E2. SPGE-E1 comprised a graphene-modified SPCE as WE with a diameter of 4 mm and SPCE-E2 had a SPCE as WE with a diameter of 3 mm. The potential windows covering both redox peaks of K$_3$Fe(CN)$_6$, DA and HQ were found to be −0.3 to + 0.6 V, −0.2 to + 0.6 V and −0.4 to + 0.6 V, respectively.

3. Results and discussion

3.1. Optimization of electrode geometries

Fig. 2A, 2B and 2C displays the effects of three geometric parameters including overall electrode length, and WE and CE active areas on the CV response of SPGEs towards 2.5 mM K$_3$Fe(CN)$_6$ in 0.1 M PBS solution (pH 7.4) at 50 mVs^{-1}, respectively. Apparently, all SPGEs exhibit reversible redox peaks due to the oxidation and reduction of (Fe(CN)$_6$)$^{3-/4-}$ couple. The anodic and cathodic peaks exhibit similar behaviors and only anodic peak current will be used for subsequent discussion. From Fig. 2A, the baseline-subtracted anodic current density (J_p) of SPGE increases from 0.20 to 0.25 mA cm^{-2} while the peak-to-peak potential separation ($\Delta E_p = E_{pc} - E_{pa}$ at 50 mVs^{-1} and 25 °C) decreases significantly from 259 to 158 mV as the overall electrode length decreases from 50 to 25 mm (Designs (a)-(b)). The behaviors can be ascribed to the decrease of electrode resistance and potential drop with decreasing electrode length. For Fig. 2B, J_p decreases from 0.26 to 0.24 mA cm^{-2} while ΔE_p increases slightly from 194 to 210 mV and the peak potentials positively shift by ~ 0.13 V as the CE active area decreases from 15.7 to 4.5 mm^2 (Designs (c)-(d)). The observed effects can be described by the role of CE on supporting the redox reactions at WE. The CE active area of 4.5 mm^2 is smaller than the WE active area of 7.1 mm^2, resulting in limited redox current and high overpotential. In the later design, CE active area of 15.7 mm^2 is slightly more than twice as large as that of WE to ensure sufficient current flow through CE. In the case of Fig. 2C, J_p increases from 0.25 to 0.30 mA cm^{-2} when ΔE_p tends to decrease from 158 to 122 mV as the WE active area increases from 4.24 to 12.57 mm^2 (Designs (b)-(c) and (e)). The attained results may be

ascribed to the reduced electrolyte resistance and potential drop between electrodes due to the decrease of the distance between WE and CE or RE from 1.5 mm to 1.05 mm with increasing WE area from 4.24 to 12.57 mm^2 [27]. The electrochemical characteristics of all designed electrodes are additionally compared with the theoretical ones by determining their electrochemical surface areas (ESAs) from the CV currents using the Randles–Sevcik equation ($I_p = KACn^{3/2}(Dv)^{1/2}$, where K = 2.69 × 10^{5}C V$^{-1/2}$ mol^{-1}, A = ESA (cm^2), C = concentration (mol·cm^{-3}), n = number of electron per reaction (=1 for Fe$^{3+/4+}$), v = scan rate (Vs^{-1}) and D = diffusion constant (=7.67 × 10^{-6} cm^{2}s^{-1} for K$_4$Fe(CN)$_6$)) as presented together with J_p in Fig. 2D. It reveals that the ESAs of Designs (c) and (e) are higher than their geometric surface areas (GSAs) while those of other designs are lower than their GSAs. It shall be noted that the CE active area of Design (e) is larger than the WE area but smaller than twice of WE area due to the physical limitation. Nevertheless, Design (e) gives superior CV peak currents and ESA to Design (c), indicating that the CE area is still adequate under the employed CV conditions. Consequently, Design (e) is considered as an optimal design and is chosen for development of SPIL-GEs.

3.2. Effects of IL type and IL content on electrochemical response of SPIL-GEs

The electrochemical performance of SPIL-GEs with six IL materials including PMPlm, BMIMBF$_4$, HMIMPF$_6$, C$_9$H$_{15}$N$_3$S, EMIMBF$_4$ and BMIMPF$_6$ have been evaluated by CV towards 5 mM K$_3$Fe(CN)$_6$ in 0.1 M PBS solution (pH 7.4) and compared with SPCE and SPGE as presented in Fig. 3A. It shows that the addition of IL remarkably enhances the redox peak amplitude towards K$_3$Fe(CN)$_6$ with insignificant changes of peak potential and the enhancement depends considerably on the IL material. The corresponding anodic peak amplitudes along with ESAs calculated using Randles–Sevcik are separately plotted in order to compare the differences among all electrodes as shown in Fig. 3B. Apparently, the oxidation peak currents and ESAs of the SPIL-GEs and SPGE are considerably higher than those of SPCE. In addition, the SPIL-GE with PMPlm exhibits remarkably high anodic peak current and ESA compared with the SPIL-GEs employing SPHMIMPF$_6$, SPC$_9$H$_{15}$N$_3$S, SPBMIMBF$_4$, SPBMIMPF$_6$, and SPEMIMBF$_4$, respectively.

From the results, the electrochemical currents are collaboratively enhanced by adding small amounts of graphene and ILs into CP. The enhancement of electrochemical response by graphene can be attributed to the improvement of electrical conductivity and effective surface area [3,6]. The insertion of highly conductive graphene sheets between carbon nanoparticles can enhance local conductivity and electron transfer rates with electroactive species. Additionally, the graphene insertion can reduce agglomeration among carbon nanoparticles, resulting in an increase of ESA in agreement with the calculated results in Fig. 3B. Concerning the roles of ILs, the enhancement of electrochemical response may be related to three main effects including electrical conductivity, electrocatalytic activity and surface wetting properties of ILs. Firstly, high electrical conductivity of IL materials distributed on graphene and carbon nanoparticles can enhance the electron transfer rates of redox processes [28–30]. Secondly, the wetting behaviors of ILs may shield graphene sheets from stacking interactions due to van der Waals forces [31], resulting in superior graphene dispersion within CP and additional electrode surface area. Lastly, ILs may catalyze the redox reactions of (Fe(CN)$_6$)$^{3-/4-}$ couple via their inherent electrocatalytic activities [32–34] imparted onto graphene and carbon nanoparticles, leading to substantial enhancement of electrochemical response with small amount of ILs. From Fig. 3C, the calculated ESA values of SPIL-GEs are remarkably higher than the GSA value. Such large extra surface areas cannot be attained only by improved graphene dispersion in the composite via ILs because of physical limitation. Thus, the electrocatalytic effect of ILs is most likely the dominant mechanism responsible for the extraordinarily large ESAs. In particular, PMPlm may exhibit higher electrocatalytic activity and better wetting capability
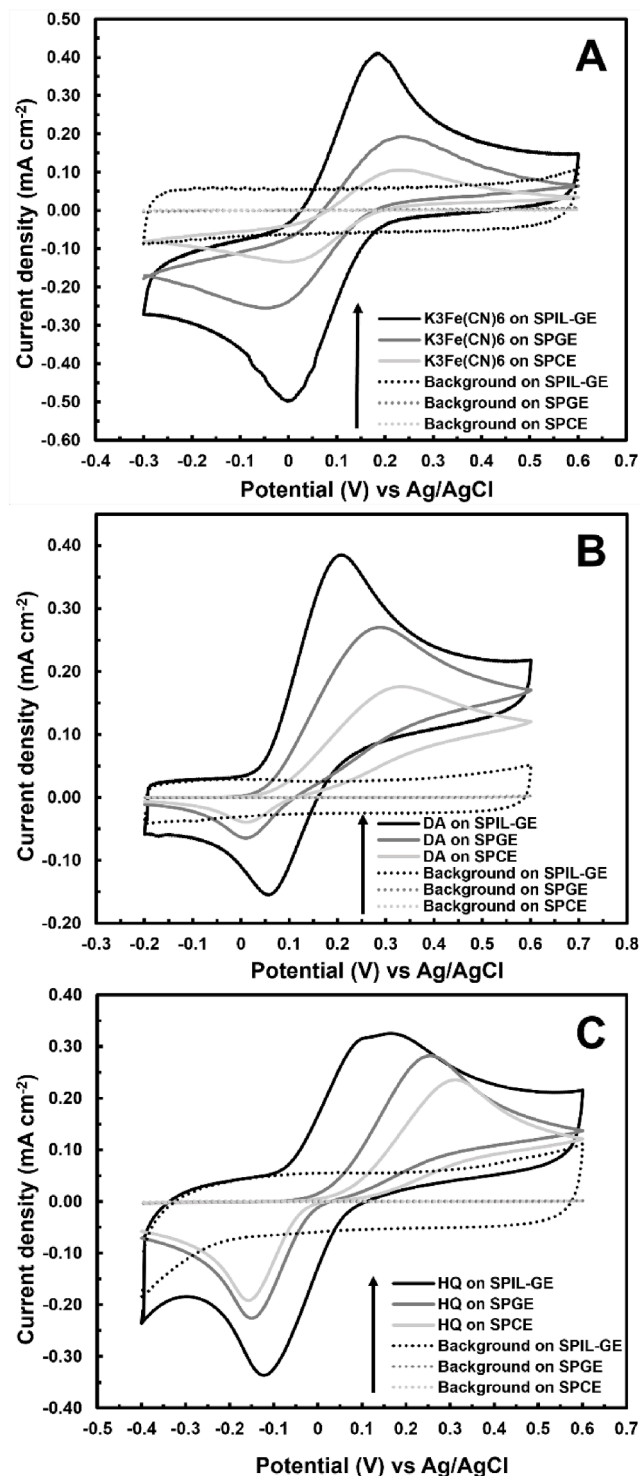
Fig. 4. Cyclic voltammograms of SPIL-GE, SPGE, and SPCE towards (a) 2.5 mM K$_3$Fe(CN)$_6$, (b) 1 mM dopamine (DA) and (c) 1 mM hydroquinone (HQ) at 50 mVs^{-1}.

with graphene surfaces than those of the five imidazolium-type ILs owing to its unique pyridinium cationic structure containing N-doped benzene ring [35], providing relatively high electrocatalytic activity and large number of electroactive sites.

The effect of PMPlm content ranging from 0.5 to 2.0 % (w/w) on the CV response and anodic signals along with estimated ESAs of SPPMPlm-GEs towards 2.5 mM K$_3$Fe(CN)$_6$ are reported in Fig. 3C and 3D,
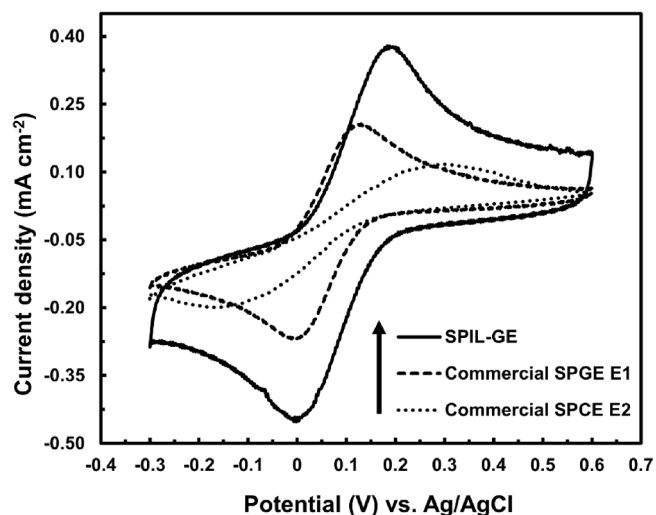
Fig. 5. Cyclic voltammograms of SPIL-GE and two commercial SPGE E1 and SPCE E2 towards 2.5 mM $K_3Fe(CN)_6$ at 50 mVs^{-1}.

respectively. The results show that the anodic peak signal and ESA increase considerably with increasing PMPlm content from 0.5 to 1.0% (w/w) but become declining when the PMPlm content increases further to 2.0 %, yielding the optimal PMPlm content of 1.0 % (w/w). The increase of CV response with increasing PMPlm content up to 1.0 % shall be ascribed to the enhanced electrocatalytic and wetting effects due to increasing distribution of PMPlm materials. However, PMPlm materials may agglomerate among themselves at PMPlm contents higher than 1.0 %, resulting in poor dispersion of PMPlm materials and reduced electrocatalytic activity as well as wetting capability. It shall be noted that the anodic peak signal and ESA in Fig. 3C and 3D are lower than that of PMPlm in Fig. 3A and 3B due to the lower $K_3Fe(CN)_6$ concentration.

3.3. Electrochemical performance of SPIL-GEs towards $K_3Fe(CN)_6$, DA and HQ

The electrochemical performance of the optimal SPIL-GE with 1% PMPlm have been evaluated and compared with those of SPGEs and SPCEs by CV measurements in 2.5 mM $K_3Fe(CN)_6$, 1 mM DA, and 1 mM HQ solutions as shown in Fig. 4A-4C, respectively. Noticeably, the SPIL-GE displays higher current with lower ΔE_p for all the three analytes than those of SPGE and SPCE. However, IL and GP provide relatively low enhancement of quasi-reversible redox reactions towards DA and HQ due likely to limited electrocatalytic activities on these large molecules.
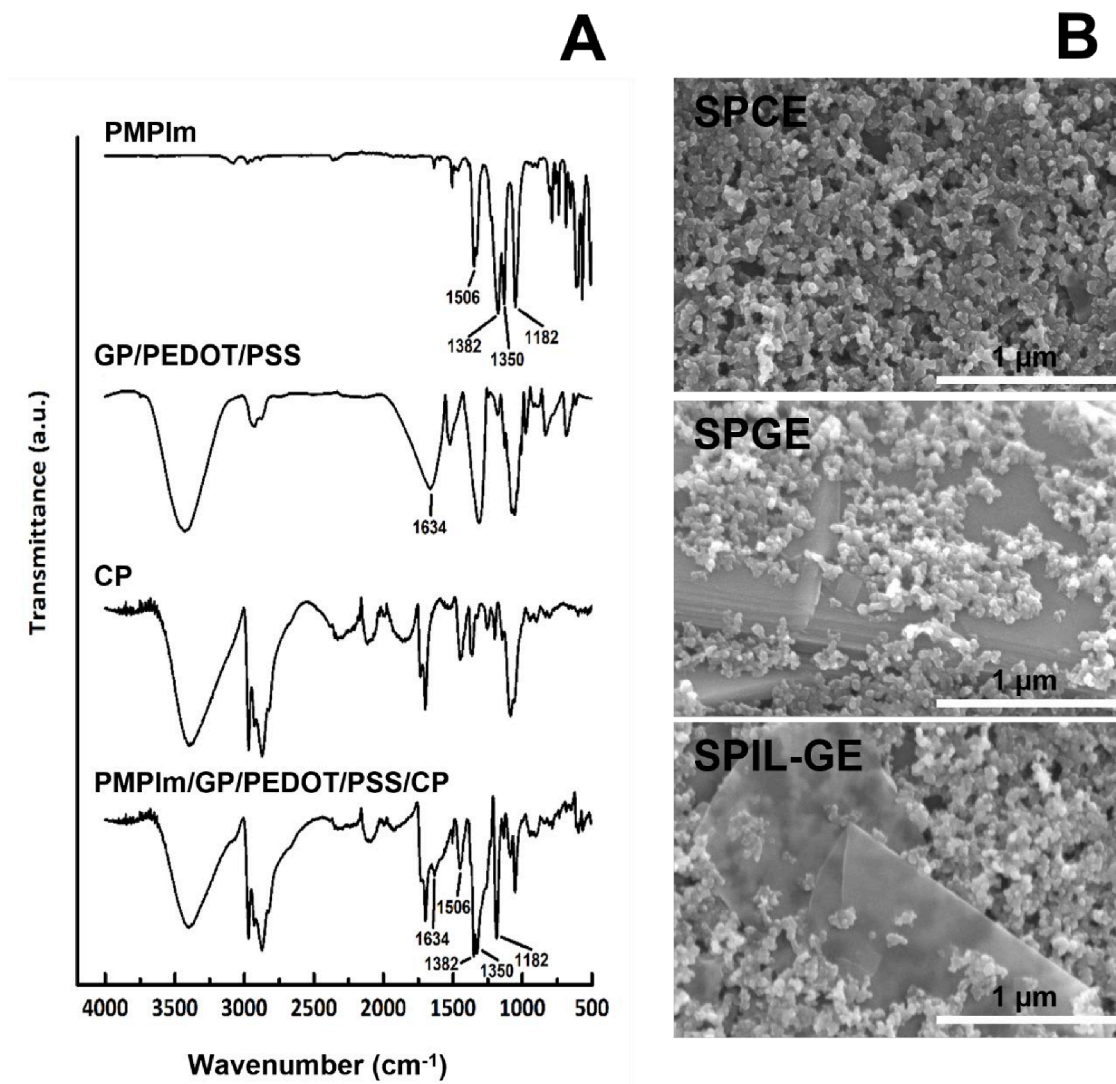
Fig. 6. (A) FTIR spectra of PMPlm, GP/PEDOT/PSS, CP and PMPlm/GP/PEDOT/PSS/CP. (B) SEM micrographs of SPCE, SPGE and SPIL-GE.

Furthermore, the optimal SPIL-GE produces higher CV peak currents towards 2.5 mM $K_3Fe(CN)_6$ than those of two selected commercial electrodes (E1: graphene modified SCPE and E2: SCPE) as demonstrated in Fig. 5. The superior redox peak currents of SPIL-GE over the commercially available graphene-modified SCPE and unmodified SCPE affirm the beneficial roles of IL and graphene on electrochemical sensing.

3.4. Structural characteristics of SPIL-GE

The chemical constituents of SPIL-GE with the optimal IL (PMPlm) have been verified using FTIR spectroscopy by comparing with the spectra of its components including PMPlm, GP/PEDOT/PSS, and CP as shown in Fig. 6A. The characteristic absorption spectrum of SPIL-GE exhibits the stretching vibrations of PMPlm comprising C-F band at 1182 cm^{-1}, S = O bands at 1350–1382 cm^{-1} and C–C band at 1506 cm^{-1}, along with the characteristic peaks of GP/PEDOT/PSS and CP, which contain C = C band at 1634 cm^{-1} and other minor bands from organic additives. The results confirm that the SPIL-GE is composed of PMPlm, GP/PEDOT/PSS and CP.

The surface morphologies of SPCE, SPGE, and SPIL-GE characterized by SEM are displayed in Fig. 6B. It shows that SPCE exhibits a porous surface consisting of connected nanoparticles with interparticle voids while SPGE and SPIL-GE contain additional nanosheets inserted between nanoparticles. The nanosheets have relatively large lateral sizes (~500–1000 nm in width and length) but are thin enough for electrons to partially see through as observed in Fig. 6B: SPIL-GE, implying that they are few-layer graphene.

4. Conclusions

SPIL-GEs were developed using conductive inks produced by adding graphene and ILs into commercial CP. Geometries of electrodes were optimized by CV measurements towards $(Fe(CN)_6)^{3-/4-}$ for SPGEs with varying overall electrode lengths, and WE and CE active areas. From the CV results, the optimal design had the overall length of 25 mm, and the WE and the CE active areas of 12.57 and 15.7 mm^2, respectively. The electrochemical response of SPIL-GEs utilizing six IL materials including PMPlm, BMIMBF$_4$, HMIMPF$_6$, C$_9$H$_{15}$N$_3$S, EMIMBF$_4$ and BMIMPF$_6$ were evaluated towards $K_3Fe(CN)_6$. PMPlm was found to yield the highest CV peak currents compared with those of other ILs at the optimal PMPlm content of 1.0% (w/w). The electrochemical response of the optimal SPIL-GE tested towards three common electroactive analytes including $(Fe(CN)_6)^{3-/4-}$ redox couple, DA and HQ were compared with SPCEs and SPGEs. The results demonstrated that SPIL-GE offered larger oxidation currents with lower anodic potentials for the three analytes than SPGE and SPCE. Therefore, the SPIL-GE could be a promising candidate for advanced electrochemical sensing applications.

CRediT authorship contribution statement

Wichayaporn Kamsong: Investigation, Methodology, Writing – original draft. **Vitsarut Primpray:** Investigation. **Patiya Pasakon:** Investigation, Writing – original draft. **Chakrit Sriprachuabwong:** Investigation. **Saithip Pakapongpan:** Investigation. **Johannes Philipp Mensing:** Writing – review & editing. **Anurat Wisitsoraat:** Writing – review & editing. **Adisorn Tuantranont:** Supervision. **Chanpen Karuwan:** Conceptualization, Methodology, Supervision, Funding acquisition, Project administration, Writing – review & editing.

Declaration of Competing Interest

The authors declare that they have no known competing financial interests or personal relationships that could have appeared to influence the work reported in this paper.

References

[1] A. Ambrosi, C.K. Chua, N.M. Latiff, A.H. Loo, C.H.A. Wong, A.Y.S. Eng, et al., Graphene and its electrochemistry – an update, Chem Soc. Rev. 45 (2016) 2458–2493, https://doi.org/10.1039/C6CS00136J.

[2] M. Pumera, Graphene-based nanomaterials and their electrochemistry, Chem Soc. Rev. 39 (2010) 4146–4157, https://doi.org/10.1039/C002690P.

[3] C. Karuwan, A. Wisitsoraat, D. Phokharatkul, C. Sriprachuabwong, T. Lomas, D. Nacapricha, et al., A disposable screen printed graphene–carbon paste electrode and its application in electrochemical sensing, RSC Adv. 3 (2013) 25792–25799, https://doi.org/10.1039/C3RA44187C.

[4] P. Pasakon, J.P. Mensing, D. Phokaratkul, C. Karuwan, T. Lomas, A. Wisitsoraat, et al., A high-performance, disposable screen-printed carbon electrode modified with multi-walled carbon nanotubes/graphene for ultratrace level electrochemical sensors, J. Appl. Electrochem. 49 (2019) 217–227, https://doi.org/10.1007/s10800-018-1268-1.

[5] C. Karuwan, A. Wisitsoraat, P. Chaisuwan, D. Nacapricha, A. Tuantranont, Screen-printed graphene-based electrochemical sensors for a microfluidic device, Anal Methods 9 (2017) 3689–3695, https://doi.org/10.1039/C7AY00379J.

[6] A. Wisitsoraat, S. Pakapongpan, C. Sriprachuabwong, D. Phokharatkul, P. Sritongkham, T. Lomas, et al., Graphene–PEDOT:PSS on screen printed carbon electrode for enzymatic biosensing, J. Electroanal. Chem. 704 (2013) 208–213, https://doi.org/10.1016/j.jelechem.2013.07.012.

[7] C. Li, G. Shi, Synthesis and electrochemical applications of the composites of conducting polymers and chemically converted graphene Electrochim. Acta 56 (2011) 10737-10743. DOI:101016/jelectacta201012081.

[8] W. Yang, Y. Zhao, X. He, Y. Chen, J. Xu, S. Li, et al., Flexible conducting polymer/reduced graphene oxide films: synthesis, characterization, and electrochemical performance, Nanoscale ResLett. 10 (2015) 222, https://doi.org/10.1186/s11671-015-0932-1.

[9] Y. Xue, H. Zhao, Z. Wu, X. Li, Y. He, Z. Yuan, The comparison of different gold nanoparticles/graphene nanosheets hybrid nanocomposites in electrochemical performance and the construction of a sensitive uric acid electrochemical sensor with novel hybrid nanocomposites, Biosens Bioelectron. 29 (2011) 102–108, https://doi.org/10.1016/j.bios.2011.08.001.

[10] P. Gupta, A. Bharti, N. Kaur, S. Singh, N. Prabhakar, An electrochemical aptasensor based on gold nanoparticles and graphene oxide doped poly(3,4-ethylenedioxythiophene) nanocomposite for detection of MUC1, J. Electroanal. Chem. 813 (2018) 102–108, https://doi.org/10.1016/j.jelechem.2018.02.014.

[11] C.A. Donini, M.K.L. da Silva, R.P. Simões, I. Cesarino, Reduced graphene oxide modified with silver nanoparticles for the electrochemical detection of estriol, J. Electroanal. Chem. 809 (2018) 67–73, https://doi.org/10.1016/j.jelechem.2017.12.054.

[12] A. a. M. Noor, P. Rameshkumar, N. Yusoff, H. N. Ming, M. S. Sajab, Microwave synthesis of reduced graphene oxide decorated with silver nanoparticles for electrochemical determination of 4-nitrophenol Ceram. 42 (2016) 18813-18820. 10.1016/j.ceramint.2016.09.026.

[13] F. Valentini, D. Roscioli, M. Carbone, V. Conte, B. Floris, E.M. Bauer, et al., Graphene and ionic liquids new gel paste electrodes for caffeic acid quantification, Sens Actuators B Chem. 212 (2015) 248–255, https://doi.org/10.1016/j.snb.2015.02.033.

[14] R. Liu, C. Lei, T. Zhong, L. Long, Z. Wu, S. Huan, et al., A graphene/ionic liquid modified selenium-doped carbon paste electrode for determination of copper and antimony, Anal Methods 8 (2016) 1120–1126, https://doi.org/10.1039/C5AY02945G.

[15] M. Shabani-Nooshabadi, M. Roostaee, F. Tahernejad-Javazmi, Graphene oxide/NiO nanoparticle composite-ionic liquid modified carbon paste electrode for selective sensing of 4-chlorophenol in the presence of nitrite, J. Mol. Liq. (2020), 114687, https://doi.org/10.1016/j.molliq.2020.114687.

[16] M. Mazloum-Ardakani, A. Khoshroo, L. Hosseinzadeh, Application of graphene to modified ionic liquid graphite composite and its enhanced electrochemical catalysis properties for levodopa oxidation, Sens Actuators B Chem. 204 (2014) 282–288, https://doi.org/10.1016/j.snb.2014.07.069.

[17] M. Du, T. Yang, S. Ma, C. Zhao, K. Jiao, Ionic liquid-functionalized graphene as modifier for electrochemical and electrocatalytic improvement: comparison of different carbon electrodes, Anal Chim. Acta 690 (2) (2011) 169–174, https://doi.org/10.1016/j.aca.2011.01.051.

[18] F. Valentini, D. Roscioli, M. Carbone, V. Conte, B. Floris, G. Palleschi, et al., Oxidized graphene in ionic liquids for assembling chemically modified electrodes:

a structural and electrochemical characterization study, Anal Chem. 84 (2012) 5823–5831, https://doi.org/10.1021/ac301285e.

[19] P. Kubisa, Ionic liquids in the synthesis and modification of polymers, J Polym Sci A Polym Chem. 43 (20) (2005) 4675–4683, https://doi.org/10.1002/pola.20971.

[20] S.K. Singh, A.W. Savoy, Ionic liquids synthesis and applications: An overview, J. Mol. Liq. 297 (2020) 112038, https://doi.org/10.1016/j.molliq.2019.112038.

[21] A.J. Greer, J. Jacquemin, C. Hardacre, Industrial Applications of Ionic Liquids Molecules 25 (2020) 5207.

[22] M. Watanabe, M.L. Thomas, S. Zhang, K. Ueno, T. Yasuda, K. Dokko, Application of Ionic Liquids to Energy Storage and Conversion Materials and Devices, Chem Rev. 117 (2017) 7190–7239, https://doi.org/10.1021/acs.chemrev.6b00504.

[23] S. Tajik, M. A. Taher, H. Beitollahi, The first electrochemical sensor for determination of mangiferin based on an ionic liquid–graphene nanosheets paste electrode Ion. 20 (2014) 1155-1161. 10.1007/s11581-013-1063-2.

[24] M.Z.M. Nasir, M. Pumera, Impact electrochemistry on screen-printed electrodes for the detection of monodispersed silver nanoparticles of sizes 10–107 nm, Phys Chem. Chem. Phys. 18 (2016) 28183–28188, https://doi.org/10.1039/C6CP05463C.

[25] A. Geto, J.S. Noori, J. Mortensen, W.E. Svendsen, M. Dimaki, Electrochemical determination of bentazone using simple screen-printed carbon electrodes, Environ Int. 129 (2019) 400–407, https://doi.org/10.1016/j.envint.2019.05.009.

[26] K. Mistry, T. Sagarika, C. Chau, H. Saha, Electrochemical Characterization of some Commercial Screen-Printed Electrodes in Different Redox Substrates Curr. Sci 109 (2015) 1427. 10.18520/v109/i8/1427-1436.

[27] F. Zhang, J. Liu, I. Ivanov, M.C. Hatzell, W. Yang, Y. Ahn, et al., Reference and counter electrode positions affect electrochemical characterization of bioanodes in different bioelectrochemical systems, Biotechnology and Bioengineering 111 (2014) 1931–1939, https://doi.org/10.1002/bit.25253.

[28] F. Valentini, D. Roscioli, M. Carbone, V. Conte, B. Floris, E.M. Bauer, et al., Graphene and ionic liquids new gel paste electrodes for caffeic acid quantification, Sensors and Actuators B: Chemical 212 (2015) 248–255, https://doi.org/10.1016/j.snb.2015.02.033.

[29] O. Zech, A. Stoppa, R. Buchner, W. Kunz, The Conductivity of Imidazolium-Based Ionic Liquids from (248 to 468) K. B. Variation of the Anion, Journal of Chemical & Engineering Data 55 (2010) 1774–1778, https://doi.org/10.1021/je900793r.

[30] A. Stoppa, O. Zech, W. Kunz, R. Buchner, The Conductivity of Imidazolium-Based Ionic Liquids from (−35 to 195) °C. A. Variation of Cation's Alkyl Chain, Journal of Chemical & Engineering Data 55 (2010) 1768–1773, https://doi.org/10.1021/je900789j.

[31] F. Valentini, D. Roscioli, M. Carbone, V. Conte, B. Floris, G. Palleschi, et al., Oxidized Graphene in Ionic Liquids for Assembling Chemically Modified Electrodes: A Structural and Electrochemical Characterization Study, Analytical Chemistry 84 (2012) 5823–5831, https://doi.org/10.1021/ac301285e.

[32] N. Maleki, A. Safavi, F. Tajabadi, Investigation of the Role of Ionic Liquids in Imparting Electrocatalytic Behavior to Carbon Paste Electrode, Electroanalysis 19 (2007) 2247–2250, https://doi.org/10.1002/elan.200703952.

[33] M. Mazloum-Ardakani, A. Khoshroo, L. Hosseinzadeh, Application of graphene to modified ionic liquid graphite composite and its enhanced electrochemical catalysis properties for levodopa oxidation, Sensors and Actuators B: Chemical 204 (2014) 282–288, https://doi.org/10.1016/j.snb.2014.07.069.

[34] Z. Wang, H. Wang, Z. Zhang, G. Liu, Electrochemical determination of lead and cadmium in rice by a disposable bismuth/electrochemically reduced graphene/ionic liquid composite modified screen-printed electrode, Sensors and Actuators B: Chemical 199 (2014) 7–14, https://doi.org/10.1016/j.snb.2014.03.092.

[35] D.i. Wei, A. Ivaska, Applications of ionic liquids in electrochemical sensors, Analytica Chimica Acta 607 (2) (2008) 126–135, https://doi.org/10.1016/j.aca.2007.12.011.